

## Original Article

# La<sub>0.6</sub>Sr<sub>0.4</sub>Co<sub>0.2</sub>Fe<sub>0.8</sub>O<sub>3- $\alpha$</sub> (LSCF) biosensor for diagnosing colorectal cancer: A quaternary alloy on an interdigitated electrode

Rong Yan<sup>a</sup>, Thangavel Lakshmi priya<sup>b</sup>, Subash C.B. Gopinath<sup>c,d,e,f,\*</sup>, Ismariza Ismail<sup>c</sup>, Sreeramanan Subramaniam<sup>c,f,g</sup>, Yeng Chen<sup>h</sup>

<sup>a</sup>Department of Surgical Oncology, First Affiliated Hospital of Xi'an Jiaotong University, Xi'an, 710061, China

<sup>b</sup>Center for Global Health Research, Saveetha Medical College & Hospital, Saveetha Institute of Medical and Technical Sciences, Thandalam, Chennai 602105, Tamil Nadu, India

<sup>c</sup>Faculty of Chemical Engineering & Technology, 02600 Arau, and Institute of Nano Electronic Engineering, 01000 Kangar, Universiti Malaysia Perlis (UniMAP), Perlis, Malaysia

<sup>d</sup>Department of Technical Sciences, Western Caspian University, Baku AZ 1075, Azerbaijan

<sup>e</sup>Department of Computer Science and Engineering, Faculty of Science and Information Technology, Daffodil International University, Daffodil Smart City, Dhaka 1216, Bangladesh

<sup>f</sup>Centre for Chemical Biology, Universiti Sains Malaysia, Bayan Lepas, 11900 Penang, Malaysia

<sup>g</sup>School of Biological Sciences, Universiti Sains Malaysia, Georgetown, 11800 Penang, Malaysia

<sup>h</sup>Department of Oral and Craniofacial Sciences, Faculty of Dentistry, Universiti Malaya, Kuala Lumpur 50603, Malaysia

## ARTICLE INFO

### Keywords:

Aptamer  
Biomarker  
Gastrointestinal cancer  
Metal alloy  
Nanosensor

## ABSTRACT

Colorectal cancer (CRC) is a type of gastrointestinal cancer affecting the colon and rectum. It can metastasize to other parts of the body, making treatment more challenging. Early identification and treatment of CRC significantly enhance patient survival rates. Therefore, the development of a suitable biosensor to monitor CRC is crucial for early diagnosis. Interleukin-6 (IL-6) is recognized as a biomarker for CRC, with elevated levels correlating to tumor progression. A highly sensitive La<sub>0.6</sub>Sr<sub>0.4</sub>Co<sub>0.2</sub>Fe<sub>0.8</sub>O<sub>3- $\alpha$</sub>  (LSCF) based interdigitated microelectrode (IDME) sensor was developed to quantify IL-6 levels. This sensor utilizes an aptamer-conjugated gold nanoparticle (GNP), which is attached to the LSCF-modified IDME through an amine linker. This step facilitates IL-6 quantification using an anti-IL-6 aptamer and antibody. The combination of LSCF and GNP significantly enhanced aptamer immobilization on the IDME, enabling the detection of IL-6 at concentrations as low as 1 pg/mL. Furthermore, IL-6 was successfully detected in serum spiked with IL-6 without interference, demonstrating the sensor's selectivity. The sensor showed no significant current responses when tested with complementary aptamers, CSE, or globulin, further confirming its specificity. Additionally, the same surface functionalization was successfully applied on an Ethylene diamine tetraacetic acid (ELISA) plate for IL-6 detection.

## 1. Introduction

Colorectal/colon cancer (CRC) is a type of gastrointestinal cancer that originates from polyps located inside the colon or rectum [1]. In its advanced stages, this type of cancer spreads beyond the bowel to other parts of the body. CRC patients are usually diagnosed at an advanced stage at which the cancer has spread and developed secondary tumors, leading to high mortality [2]. Patients in the early stages of CRC often do not show obvious symptoms, such as abdominal pain or gastrointestinal bleeding, and it can take years or even decades for a diagnosis to be made. Despite CRC being a relatively straightforward surgical case that can benefit from postoperative chemotherapy, it still has a poor five-year survival rate. Therefore, developing sensitive, efficient, and compliant detection technologies is crucial for diagnosing CRC early and increasing the chances of successful treatment and intervention [3]. Currently, endoscopy, stool analysis, tumor biomarker detection, and imaging are the most commonly used clinical techniques for CRC detection. Blood biomarkers, a non-invasive method for CRC screening,

have shown significant potential for early cancer diagnosis, prognosis, prediction, and staging [4].

A pioneering biosensing technique has been effectively utilized for the prognosis of CRC by measuring biological markers involved in the development of the disease. Research has shown that pro-inflammatory cytokines play a significant role in tumor formation, particularly the pleiotropic cytokine interleukin-6 (IL-6), which is strongly linked to inflammation-associated CRC. IL-6 is very involved in both inflammation and immune responses. It plays a major role in autoimmune diseases, chronic inflammatory diseases, and cancers. Elevated levels of IL-6 were found in various inflammatory diseases, such as arthritis, Crohn's disease, and ankylosing spondylitis. The level of IL-6 is less than 5 pg/mL in normal patients and increases drastically during infection, inflammation, cancer, and injuries. IL-6 is an inflammatory cytokine, and its downstream effector, STAT3, is involved in the proliferation of CRC, cell cycle progression, invasion and metastasis, stemness, and tumorigenesis [5,6]. The mean serum level of IL-6 was 88.22 pg/mL in CRC patients, which was much higher than the control group [7]. Further,

### \*Corresponding author:

E-mail address: [subash@unimap.edu.my](mailto:subash@unimap.edu.my) (S.C.B. Gopinath)

Received: 30 October, 2024 Accepted: 27 January, 2025 Published: 18 March 2025

DOI: 10.25259/AJC\_123\_2024

It was identified that the level of IL-6 was higher in CRC tissue samples. In postoperative settings, IL-6 levels are a major predictive factor for stage I–III CRC. Elevated levels of IL-6 are correlated with advanced tumor stages and lower survival rates in CRC patients. This is due to IL-6 trans-signaling, which stimulates gp130 on tumor cells, promoting growth, angiogenesis, metastasis, and resistance to treatment. According to related research, IL-6 levels in the blood and tumor tissue of CRC patients can indicate the proliferative activity of tumors and are strongly correlated with tumor stage [8]. In stage III patients, IL-6 levels have been identified as an independent risk factor for disease-free survival [8]. So, patients with bowel changes, bloody stools, and abdominal discomfort need to check their IL-6 level to identify the possibility of CRC. Additionally, during the treatment of CRC, there is a need to quantify the IL-6 level to monitor the progress. Therefore, quantifying IL-6 levels helps in identifying CRC and assessing its progression. In this study, we introduce a nanomaterial-based interdigitated microelectrode (IDME) sensor for detecting IL-6 with high sensitivity.

An extensive variety of nanomaterials with superior mechanical, chemical, and physical properties have been developed and adopted to biosensing platforms, thanks to advancements in nanoscience and nanotechnology [9,10]. The use of metal nanostructures in the creation of highly sensitive electrochemical biosensors has proven appealing. Noble metal nanostructures, such as those of Au, Ag, Pt, Pd, Ni, Fe, Si, and zeolites, have been effectively utilized in the development of biosensors to meet the growing demand for highly sensitive and selective diagnostic tools [11–13]. Due to their high surface energy, small size, and fast electron transfer, nanostructured noble metals possess exceptional qualities that significantly enhance electrochemical biosensors by facilitating electrochemical processes at the electrode–solution interface. Among individual metals, alloy-based nanomaterials offer a promising platform for developing various biomedical applications, including biosensors. They provide a larger surface area for immobilizing biological molecules, which helps to lower detection limits [14]. Additionally, metal alloys are efficient in detecting biomolecules in complex samples, promoting the selective detection of target molecules. Furthermore, nanomaterials are non-genotoxic and biocompatible, and they can be easily functionalized or encapsulated in polymers. This facilitates the creation of biosensing platforms with multiple nanomaterials, enhancing their analytical performance [15,16]. Moreover, nanomaterials have emerged as a remarkable class of nanoparticles for use as drug delivery vehicles, particularly in cancer therapies such as hyperthermia, due to their exceptional biocompatibility and low toxicity [17,18]. Alloys are a combination of two or more solid elements that can be used for different applications as they bring a combined effect of all the desired elements. In this research, molecular immobilization was enhanced using  $\text{La}_{0.6}\text{Sr}_{0.4}\text{Co}_{0.2}\text{Fe}_{0.8}\text{O}_{3-\alpha}$  (LSCF) to develop an IL-6 biosensor. This oxide material is frequently used in electrochemical devices, and its specific composition has been optimized to improve electrochemical performance and maintain stability. LSCF has been considered a potential intermediate product suitable for cathode application.

An aptamer is a single-stranded nucleic acid identified from a randomized library of molecules by a method called the ‘Systematic Evolution of Ligands by Exponential Enrichment’. This process involves binding, recovery, and amplification steps to select high-affinity molecules [19,20]. Aptamers possess unique characteristics, such as high binding affinity and specificity for their target molecules. Often referred to as artificial antibodies, aptamers can replace antibodies in various biomedical applications. Moreover, aptamers have several advantages over antibodies, including high affinity, ease of preparation, lack of variation, non-immunogenicity, and simple functionalization [21]. Aptamers bind to small regions of their target via their secondary structure, allowing them to distinguish between closely related molecules, a task that is often challenging for antibodies [22]. Due to these beneficial features, aptamers are increasingly used in biosensors to develop high-affinity sensors for early disease diagnosis [23]. Various point-of-care biosensors, including portable models, have also been developed using aptamers as probes for disease screening. In this study, an anti-IL-6 aptamer was attached to an LSCF-modified IDME to quantify IL-6 levels. To enhance aptamer immobilization, the aptamer was first conjugated to a gold nanoparticle (GNP) and then

attached to the amine-modified LSCF. The combination of aptamers and GNPs is widely popular in the biosensor field due to its versatile applications [24]. For instance, a colorimetric assay using aptamers and GNPs enables the detection of target molecules by the naked eye [25]. Beyond that, this conjugation proved to provide stable aptamer immobilization on the electrode with proper orientation, lowering the detection limit. Aptamers were conjugated to GNPs through an SH linker and immobilized on amine-modified LSCF, which was then used to quantify IL-6 levels with the immobilized aptamer and detection antibody.

## 2. Materials and Methods

### 2.1. Materials and reagents

Aluminum oxide, ethanol, acetone, positive photoresist, and resist developer (RD6) were purchased from Futurrex, Inc. Current-voltage (I-V) measurements were conducted using a Keithley 2450, assisted by a probe station and Kickstart software. carcinoembryonic antigen (CEA), tumor necrosis factor (TNF), ELISA plates, phosphate-buffered saline (PBS), IL-6, (3-Aminopropyl)triethoxysilane, and gold nanoparticle (10 nm) were obtained from Sigma-Aldrich (USA). Anti-IL-6 antibody, IgG antibody, Horseradish peroxidase (HRP)-conjugated secondary antibody, and TMB substrate were sourced from Promega (USA). The anti-IL-6 aptamer was adapted from a previous study and synthesized commercially by a local supplier [26]. [5'-SH-GGTGGCA GGAGGACTATTTATTTGCTTTTCT-3']. The sensing surface was kept wet using 10 mM PBS (pH 7.4) in order to maintain the secondary and tertiary structures of biomolecules. For the preparation of alloys,  $\text{La}(\text{NO}_3)_3 \cdot 6\text{H}_2\text{O}$ ,  $\text{Sr}(\text{NO}_3)_2$ ,  $\text{Co}(\text{NO}_3)_2 \cdot 6\text{H}_2\text{O}$  and  $\text{Fe}(\text{NO}_3)_3 \cdot 9\text{H}_2\text{O}$  were obtained from Thermo Scientific, USA. Citric acid monohydrate (CA) (MERCK, USA), Ethylene diamine tetraacetic acid (EDTA), and ethylene glycol were obtained from Thermo Scientific, USA. Charcoal-activated carbon was received from HmbG, Malaysia. The current supply was provided by picoammeter at the range of 0 to 2 V with a sweep interval of 0.1 V on a fixed dual probe station.

### 2.2. Synthesis of $\text{La}_{0.6}\text{Sr}_{0.4}\text{Co}_{0.2}\text{Fe}_{0.8}\text{O}_{3-\alpha}$ (LSCF)

The stoichiometric composition of  $\text{La}(\text{NO}_3)_3 \cdot 6\text{H}_2\text{O}$ ,  $\text{Sr}(\text{NO}_3)_2$ ,  $\text{Co}(\text{NO}_3)_2 \cdot 6\text{H}_2\text{O}$ , and  $\text{Fe}(\text{NO}_3)_3 \cdot 9\text{H}_2\text{O}$  was dissolved in 100 mL of deionized water to create the precursor solution. CA and EDTA were added to the nitrate solution after the salts had completely dissolved. The mixture was then heated in a water bath at 70°C with constant stirring. Powdered CA and EDTA were used as the starting materials for the chelation process. To promote dispersion and prevent clumping of the resulting cathode materials, dispersing agents were added to the clear solution. Two types of dispersing agents, ethylene glycol and activated charcoal, were used in the synthesis process. The mixture was continuously stirred and heated to evaporate the water. Afterward, the solidified precursor was ground and calcined at 400 to 1100°C for five hrs, following the drying of the resulting viscous gel at 100°C overnight in a vacuum oven to promote the formation of the LSCF perovskite phase.

### 2.3. IDME sensor fabrication

Using AutoCAD software, the electrode length, gap size, and thickness were first optimized. The following steps outline the fabrication and transformation process: (a) Si wafer was cleaned using RCA1 and RCA2 solutions; (b) thermal oxidation was performed at 500°C for one hour to create a layer of  $\text{SiO}_2$ ; (c) an aluminum coil was used to deposit the Al layer on  $\text{SiO}_2$  with the assistance of a thermal evaporator; (d) a positive photoresist was deposited using the spin-coating technique; (e) UV light exposure was used to transfer the pattern onto the photoresist; (f) the electrode was immersed in the photoresist developer and aluminum etching solution to remove the unexposed areas; and (g) the final product was cleaned with acetone and distilled water.

### 2.4. Gold-aptamer conjugation

The conjugation of GNP and aptamer was carried out using a thiol-linker with six carbon spacers. A solution of 0.12  $\mu\text{M}$  thiol-linked

aptamer and 50  $\mu\text{L}$  of GNP was mixed and allowed to rest for 30 mins. The aptamers bound to the GNP were collected by centrifugation at 10,000  $\times$  g for 10 mins. The conjugated material was then rinsed with distilled water to remove any unbound aptamer and separated again by centrifugation before being stored in a refrigerator for future use. Similarly, other aptamer concentrations (0.25, 0.5, 1, and 2  $\mu\text{M}$ ) were also conjugated with GNP.

### 2.5. Aptamer immobilization on IDME

Aptamer immobilization on the IDME was performed using three different methods and compared. In Method 1, the IDME was immersed in KOH for 10 mins and then rinsed with distilled water. A 1% solution of APTMS was applied to the surface and left for three hrs, followed by the addition of 1  $\mu\text{M}$  COOH-aptamer, which was allowed to rest for 30 mins. In Method 2, 1  $\mu\text{M}$  aptamer-GNP was added to the APTMS-modified IDE. All other steps were followed as described previously. In Method 3, after KOH treatment, APTMS-LSCF (1 mg/mL of LSCF dispersed in 1% APTMS, left for three hrs, and separated by centrifugation) was applied to the IDME. Then, 1  $\mu\text{M}$  Aptamer-GNP was added to the (3-Aminopropyl)trimethoxysilane (APTMS)-LSCF-modified IDME. The I-V measurements were recorded for all three methods and compared.

### 2.6. Optimization of aptamer-GNP on LSCF modified IDME

Aptamer-GNP optimization was performed on the LSCF-modified IDME. In this process, the IDME was immersed in KOH for 10 mins and then rinsed with distilled water. After the KOH treatment, APTMS-LSCF was applied to the IDME. Subsequently, Aptamer-GNP concentrations ranging from 0.12  $\mu\text{M}$  to 2  $\mu\text{M}$  were added to the APTMS-LSCF-modified IDME. After washing the surface with PBS buffer, I-V measurements were recorded for all aptamer concentrations, and the current responses were compared.

### 2.7. IL-6 interaction with aptamer and antibody

The quantification experiment for IL-6 was performed using the optimized aptamer-GNP concentration. The optimized aptamer-GNP was applied to the IDME and allowed to rest for 30 mins. Afterward, an IL-6 concentration of 0.1  $\text{pg/mL}$  was added, and the mixture was allowed to sit for another 30 mins. After washing the electrode with PBS, I-V measurements were recorded. Similarly, the other IL-6 concentrations (1, 10, 100, 1000, 2000, and 3000  $\text{pg/mL}$ ) were also measured. The differences in current responses were plotted on a linear regression line to calculate the limit of detection for IL-6. Furthermore, to ensure selective detection of IL-6, the same procedures were carried

out with IL-6-spiked human serum. Different IL-6 concentrations were diluted in serum and applied to the aptamer-GNP-modified IDME, which was then sandwiched with anti-IL-6 antibody. After washing the surface with PBS buffer, I-V measurements were recorded.

### 2.8. Specific detection of IL-6

Specific IL-6 detection performance was assessed using control proteins, namely the carcinoembryonic antigen (CEA) and tumor necrosis factor (TNF). Instead of IL-6, these two proteins were used. In another experiment, the complementary aptamer-GNP was attached to APTES-LSCF and detected using IL-6 and anti-IL-6 antibodies. Furthermore, the IgG antibody was used in the control experiments instead of the anti-IL-6 antibody. I-V measurements were recorded in all the control experiments.

Results were averaged from three independent experiments performed on three sensing surfaces fabricated from the same batch. The regression coefficient ( $R^2$ ) was calculated on a linear curve graphed on an Excel sheet. The limit of detection (LOD) was considered the lowest concentration of a target (on the calibration line) against the background signal ( $S/N = 3:1$ ). Meaning,  $\text{LOD} = \text{standard deviation of the baseline} + 3\sigma$ . All experiments were performed at room temperature (RT) and ambient humidity. Washed the interactive surface between each modification using 10 reaction volumes of 10 MM PBS (pH 7.4).

### 2.9. ELISA surface functionalization for IL-6 detection

The same surface functionalization was performed on the ELISA polystyrene plate to detect IL-6. The ELISA wells were hydroxylated with KOH, and then APTMS-LSCF was added. Subsequently, the Aptamer-GNP conjugation was introduced, followed by the addition of PEG-COOH to block the free APTMS. After that, IL-6, ranging from 0.1 to 3000  $\text{pg/mL}$ , was added to different wells and allowed to rest for 30 mins, after which the anti-IL-6 antibody was added. Finally, a secondary antibody conjugated with HRP was added, followed by the addition of the substrate for HRP. The absorbance was recorded using an ELISA reader at 405 nm.

## 3. Results and Discussion

Perovskite is a class of materials with the  $\text{ABO}_3$  crystal structure, where 'A' represents a larger cation, usually an alkaline earth metal like calcium (Ca), strontium (Sr), or lanthanum (La). 'B' stands for a smaller cation, such as iron (Fe), cobalt (Co), or titanium (Ti), which are transition metals.  $\text{O}_3$  forms an octahedral coordination around the B-site ion, enveloping the cations. The mineral  $\text{CaTiO}_3$ , named after the Russian mineralogist Lev Perovski and initially identified by

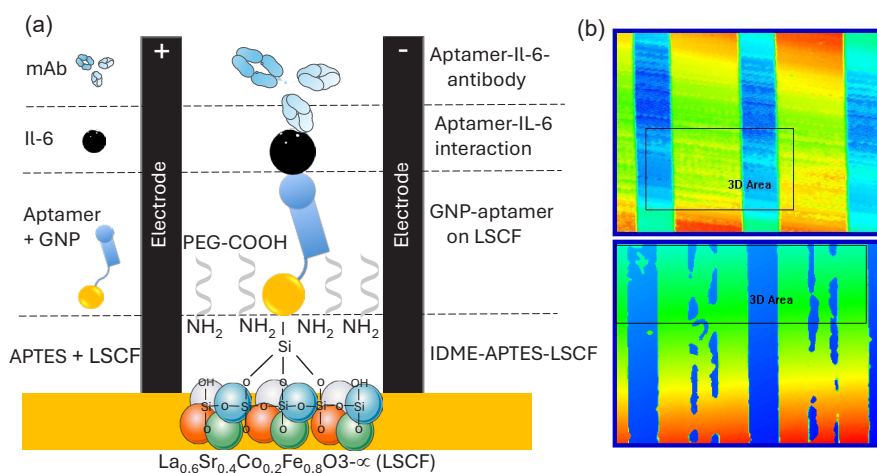


**Figure 1.** (a) Graphical illustration of the IL-6 biosensor on the  $\text{La}_{0.6}\text{Sr}_{0.4}\text{Co}_{0.2}\text{Fe}_{0.8}\text{O}_{3-x}$ -gold nanoparticle (LSCF-GNP) modified interdigitated microelectrode (IDME). The electrode was hydroxylated with KOH and then modified with (3-Aminopropyl)trimethoxysilane)- $\text{La}_{0.6}\text{Sr}_{0.4}\text{Co}_{0.2}\text{Fe}_{0.8}\text{O}_{3-x}$  [APTMS-LSCF]. Aptamer-GNP conjugation was applied, followed by the addition of IL-6. Finally, the immobilized IL-6 was sandwiched with the anti-IL-6 antibody. (b) 3D nanoprofiler observations are shown. The upper panel displays observations before molecular attachment, while the lower panel shows the results after molecular attachment.

Gustav Rose in 1839, is the origin of the term “perovskite.” However, a broad variety of materials with the same crystal structure but distinct chemical compositions are also referred to as perovskites. The ability of perovskite oxides to selectively permit ion flow makes them useful in sensors. This study utilizes LSCF-mediated sensors to monitor the condition of CRC. Figure 1(a) shows a graphical illustration of the IL-6 biosensor on LSCF-GNP modified IDME. To improve the sensitivity of the affinity-based biomolecular interactions, an aluminum-modified electrode was preferred for better conductivity. The electrode was hydroxylated with KOH, which enhanced the amine modification. On the amine-modified IDME, aptamer-GNP conjugation was applied, followed by the addition of IL-6. Finally, the immobilized IL-6 was sandwiched with the anti-IL-6 antibody. LSCF and GNP increase the aptamer attachment on the IDME and enhance the detection of IL-6. The surface intactness and the molecular attachment were confirmed by imaging under 3D-nanoprofiler (Figure 1b).

### 3.1. Characterization of LSCF

The shape and size of the LSCF were identified using Field Emission Scanning Electron Microscopy (FESEM) (Figure 2), showing a magnitude of 500 nm. The nanoparticles are spherical, with a diameter ranging between 15 and 60 nm. Furthermore, the nanoparticles exhibit uniform size and shape distribution. The elements in the synthesized nanoparticles were analyzed using Energy Dispersive X-ray Spectroscopy (EDX), revealing the presence of Co (34%), Sr (17%), La (26%), and Fe (23%) (Figure 2; inset).

### 3.2. Comparison of aptamer immobilization on IDME

Probe immobilization plays a vital role in improving biosensor performance. A higher number of probe molecules on the biosensor enhances target detection and lowers the detection limit. Researchers have studied various physical, chemical, and electrostatic interactions for the efficient immobilization of probe molecules. In recent decades, nanomaterials have garnered significant attention for surface functionalization in biosensor development. In this study, two nanomaterials, namely LSCF and GNP, were used to enhance the immobilization of the aptamer probe on the IDME. Figure 3(a) shows the aptamer immobilization without LSCF and GNP. As shown in the figure, the hydroxylated IDME shows the current response as  $1.07 \times 10^{-5}$  A; after APTES modification, it was increased to  $2.33 \times 10^{-5}$  A. Further, adding aptamer to the surface, the current was drastically increased to  $5.44 \times 10^{-5}$  A. This current increment is considered as the binding of aptamer-GNP on the APTS-LSCF-modified surfaces. This immobilization

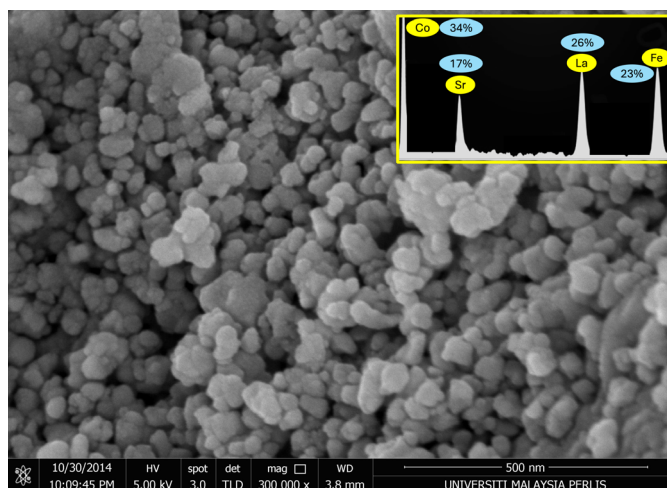


**Figure 2.** The Field Emission Scanning Electron Microscopy (FESEM) image of  $\text{La}_{0.6}\text{Sr}_{0.4}\text{Co}_{0.2}\text{Fe}_{0.8}\text{O}_{3-\alpha}$  (LSCF) shows a magnification of 500 nm, revealing nanoparticles with a uniform shape. The Energy Dispersive X-ray Spectroscopy (EDX) analysis of LSCF, displaying the presence of various alloys, is presented as an inset figure. Figure inset displays percentages of the elemental concentrations.

happened due to the binding of citrus-capped GNP with the amine in the APTES. Figure 3(b) shows the aptamer immobilization with GNP. For that, aptamer-GNP was added onto the APTES modified IDME. As shown in Figure 3(b), after adding aptamer, the current was improved to  $8.44 \times 10^{-5}$  A. Compared with the previous experiment, when aptamer was conjugated with GNP, the aptamer immobilization was almost doubled on the IDME. This was due to the higher aptamers attaching to the surface of the GNP. Various research proved that biomolecules with GNP are stable and improve the number of probes immobilization on the electrode. Apart from that, the gold nanomaterials have a higher surface area, and aptamers are smaller in size than antibodies, which improves the number of bindings of aptamers on the GNP. For instance, the strong binding of clotting FIX on the ELISA polystyrene plate was achieved through the GNP. The antibody or protein immobilization and its stability depended on the charges arising from the amino acids and the sensing surfaces. GNP conjugated FIX was stable under the high sodium concentrations, and it increased the number of FIX binding on the ELISA polystyrene (ELISA PS) well, which lowered the detection limit of FIX to 100 pM [27]. Similarly, the aptamer and antibody were attached to the single gold urchin through the chemical modification

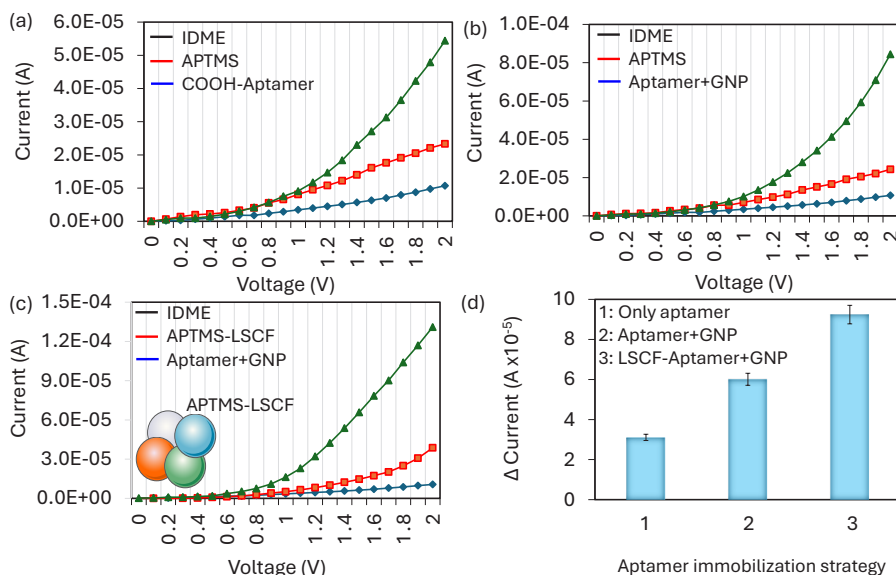


**Figure 3.** Comparison of aptamer immobilization: (a) Without GNP and LSCF, (b) With GNP, (c) With LSCF and GNP, and (d) Comparison of current responses from aptamer immobilization. The highest current level was recorded when both nanomaterials, LSCF and GNP, were used in the aptamer immobilization process.

and attached on the electrode surface to quantify the Alzheimer biomarker A $\beta$ O. Gold nano-urchin is capable of carrying out the two probes of aptamer and antibody with higher stability on the electrode, increasing the detection probe immobilization and lowering the limit of detection of A $\beta$ O for diagnosing Alzheimer's disease [28]. Due to the excellent stability of the GNP with biomolecules, in the third method, aptamer-GNP was attached to the LSCF-modified IDE (Figure 3c). Bare IDME shows the current response as 1.09 E-05 A; after modifying with APTMS-LSCF, it was increased to 3.86 E-05 A. This current change indicates that the surface was converted into amine-modified LSCF. Further, aptamer-GNP was added, and the current was changed to 1.31 E-04 A. This current increment is the highest among the previous two methods. When comparing these three methods of aptamer immobilization, the highest level of current was recorded when using both nanomaterials LSCF and GNP for the aptamer immobilization process (Figure 3d). Gold with a higher surface area enables the increment of biomolecule functionalization, whereas LSCF plays an exceptional role in transmitting the electrical signal throughout the electrodes. The application of nanocomposites has been widely reported in recent days for various biosensing applications. For instance, metal and nanocellulose crystalline conjugation was modified on the screen-printed carbon electrode for the identification of tuberculosis. The DNA biosensor was conducted. The fabricated biosensor identifies the target DNA as low as  $7.96 \times 10^{-13}$  M. In addition, the sensor can clearly differentiate between TB and non-TB samples [29]. In another study, iron and gold nanomaterial is proposed, which can simultaneously work as a reporter and at a preconcentration of a target. This dual nanomaterial improves the target DNA detection by 18 times compared to the magnetic particle in the plasmonic biosensor [30]. With this regard, the successful application of LSCF nanocomposite with GNP was used to attach higher aptamer immobilization and detection of IL-6, creating a highly sensitive biosensing platform for CRC.

### 3.3. Aptamer optimization on LSCF-GNP composites on IDME

It was identified that the combination of LSCF and GNP improves the aptamer immobilization on IDME. Different concentrations of aptamers were optimized on LSCF0-modified surfaces. Figure 4(a) shows the I-V measurement graph of different aptamer-GNP (0.12 nM to 2  $\mu$ M) immobilization on APTMS-LSCF-modified electrodes. As shown in the figure, 0.12  $\mu$ M of aptamer shows the response of current as 5.03 E-05 A, which is 1.17 E-05 increment of current from the LSCF modified electrodes. This indicates some of the APTES-LSCF surfaces were covered with Aptamer-GNP. With further increase in the aptamer-

GNP concentration to 0.25, 0.5, 1, and 2  $\mu$ M, the response of current increased to 7.57 E-05 A, 1.22 E-04 A, 1.31 E-04 A, and 1.37 E-04 A, respectively. It was noticed that the aptamer binding drastically increased at 0.5  $\mu$ M, after which gradual increment was noted, followed by saturation at 1  $\mu$ M (Figure 4b). The aptamer saturation on the GNP depends on its size. Smaller-sized particles cannot cover a higher number of biological molecules. In the previous experiment with ELISA surface modification, 10, 15, and 80 nm of GNPs were tested for antibody immobilization. It was found that 15 and 80 nm shows the same absorbance level, while 10 nm shows a lower absorbance due to the lesser attachment of antibody [27]. So, in our experiment, the median size of 30 nm of GNP was used for the aptamer immobilization. In addition, compared with antibodies, the aptamer need a smaller space on the GNP, which also increases the aptamer binding on GNP surface. In our experiment, the current response was approximately the same for 1  $\mu$ M aptamer, indicating the saturation point. A previous study also revealed that the aptamer concentration is more stable on the GNP from 1  $\mu$ M, even with the higher concentration of the salt. The optimized concentration of 1  $\mu$ M was used further for quantifying IL-6. After the confirmation of aptamer concentration, the GNP binding on aptamer was further confirmed with UV-Vis spectroscopy analysis. Figure 4(c) shows the clear shift of the spectrum to the right side with the aptamer-conjugated GNP, which confirms the immobilization of aptamer on the GNP.

### 3.4. IL-6 detection LSCF-GNP composites on IDME

The optimized aptamer-GNP was attached to the IDME, and then IL-6 was detected by the aptamer-IL-6-antibody assay. IL-6 from 0.1 to 3000 pg/mL was dropped on the aptamer immobilized surface and then sandwiched with the anti-IL-6 antibody. Figure 5(a) shows the I-V measurement graph of a different concentration of IL-6 detection. As shown in Figure 5(a), before adding IL-6, the surface current was recorded as 1.39 E-04 A; it was increased a bit to 1.67 E-04 A when adding 0.1 pg/mL of IL-6. Smaller changes of current were noted due to lesser immobilization of IL-6 with the aptamer. Further, IL-6 was increased to 1 pg/mL, the current response was almost double from the blank, which confirms the clear interaction of IL-6 with its aptamer and antibody. This current increment was due to the stable and proper orientation of the aptamer, which attracts even the lower concentration of IL-6 and enhances the current response when sandwiched with its antibody. With increasing IL-6 to 10, 100, 1000, 2000, and 3000 pg/mL, current shows increments to 2.7 E-04 A, 4.31 E-04 A, 5.81 E-04 A, 7.09 E-04 A, 9.07 E-04 A, and 12.3 E-04 A, respectively (Figure 5b). This increment

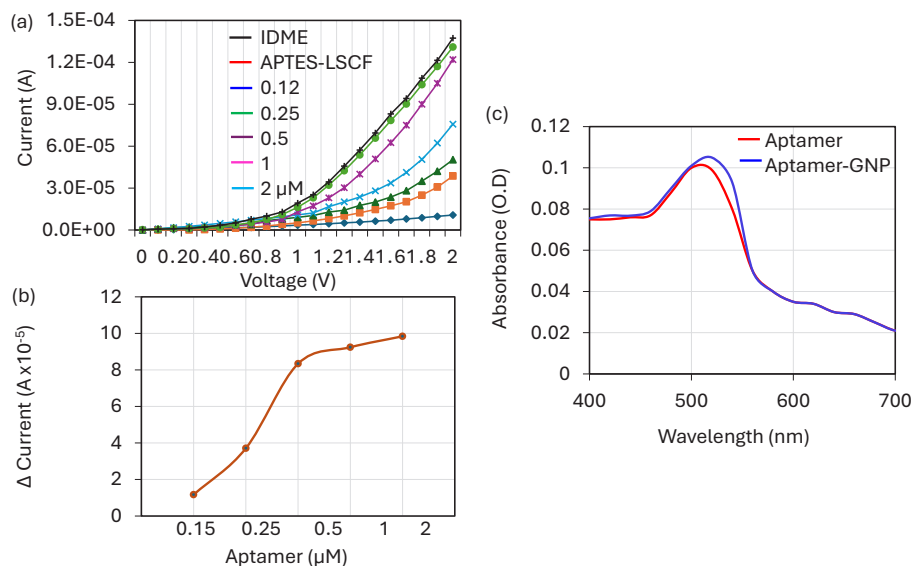


**Figure 4.** Aptamer Optimization: (a) I-V measurement graph showing different aptamer-Gold Nanoparticle (GNP) immobilizations on (3-Aminopropyl)trimethoxysilane) La<sub>0.6</sub>Sr<sub>0.4</sub>Co<sub>0.2</sub>Fe<sub>0.8</sub>O<sub>3- $\infty$</sub>  (APTMS-LSCF) modified electrodes. Changes in current responses were noted after adding each aptamer concentration. (b) Current levels of different aptamer-GNP combinations on La<sub>0.6</sub>Sr<sub>0.4</sub>Co<sub>0.2</sub>Fe<sub>0.8</sub>O<sub>3- $\infty$</sub>  (LSCF). As the concentration of aptamer-GNP increased, the current response also increased, saturating at 1  $\mu$ M. (c) UV-Vis spectroscopy of aptamer and aptamer-GNP. The shift of the spectrum to the right with the aptamer-GNP confirms the immobilization of the aptamer on the GNP.

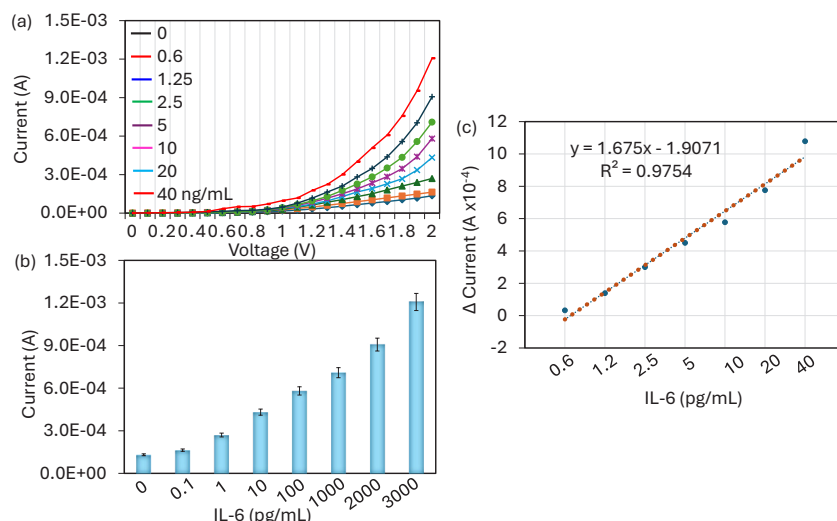


**Figure 5.** IL-6 Quantification. (a) I-V measurement graph showing the detection of different concentrations of Interleukin-6 (IL-6). Changes in current responses were noted after adding each IL-6 concentration. (b) Current levels for various IL-6 detections. As IL-6 concentration increased, the current response exhibited an increasing trend. (c) Limit of detection for IL-6. The detection limit was calculated by identifying the differences in current responses from the blank for each IL-6 concentration and plotted in an Excel spreadsheet. The detection limit was determined to be 1 pg/mL, with an  $R^2$  value of 0.9754.

of current was due to the higher IL-6 interaction with aptamer and detected by anti-IL-6 antibody. In this IL-6 biosensor, aptamer was used to capture the IL-6 due to its higher sensitivity with IL-6 than antibody. The research was proven in the sandwich assay, when aptamers were used to capture the target molecule. They specifically capture the target with higher sensitivity and improve the LOD. Previously, an A $\beta$  oligomer was detected by its aptamer and antibody on the ELISA plate. Aptamer was used to capture the A $\beta$  oligomer and detected with an anti-A $\beta$  oligomer antibody. The nanomaterial-modified ELISA well lowers the detection limit to 50 pM [31]. In another research, Lakshmi Priya *et al.* developed an influenza biosensor by using the aptamer selected against influenza B and anti-influenza B antibody. It was identified that aptamers have more potential to detect the influenza virus than antibodies [14]. Our IL-6 biosensor also shows a great increment of current responses with increasing IL-6 by using aptamer-IL-6-antibody sandwich assay. The detection limit was calculated by identifying the difference between current responses and blank for each IL-6 concentration and they were plotted in an Excel spreadsheet. The detection limit was calculated as 1 pg/mL with an  $R^2$  value of 0.9754 (Figure 5c). Similar to this experiment, researchers developed an IL-6 biosensor on GNP and platinum carbon-modified sensor with the linker of anti-IL-6 antibody. This biosensor specifically recognizes the IL-6 by using voltammetry as low as 3 pg/mL with a range of detection of 100-700 pg/mL [32]. Similarly organic electrochemical transistor biosensor was performed to quantify the level of IL-6. GNP was deposited on the poly(3,4-ethylenedioxythiophene) doped with polystyrene sulfonate gate electrode for the subsequent immobilization of SH-linked aptamers. This sensing surface shows the A detection range of IL-6 from picomolar to nanomolar range [33]. Similarly various sensors are developed by researchers for IL-6 quantification and have been summarized in Table 1.

**Table 1.** IL-6 detection with various currently available sensors

Sensor	Probe	Nanomaterial	Detection limit (pg/mL)	Reference
Voltammetry	Antibody	Carbon-GNP	3	[33]
Electrochemical transistor	Aptamer	Gold	Lower picomolar	[34]
Paper-based	Antibody	Gold nanoparticle	1.3	[35]
Cyclic voltammetry	Antibody	Biochar	0.78	[36]
Electrochemical	Antibody	ZnO	0.2	[37]
Paper-based	Antibody	Graphene	9.55	[38]
FET-sensor	Antibody	Graphene oxide	1.53	[39]
IDME	Aptamer and antibody	LSCF and GNP	1	This study

Our sensing strategy is comparable with the already existing method with a detection limit of 1 pg/mL.

### 3.5. IL-6 detection in serum spiked sample

A successful biosensor can identify targets in biological samples such as urine, serum, sweat, and blood. To mimic this situation, IL-6 (0.1-3000 pg/mL) was spiked into serum and detected using the IL-6 biosensor. In healthy individuals, the IL-6 level is typically less than 6 pg/mL. The IL-6 level in serum is highly correlated with tumor stages in CRC, with the mean tumor level of IL-6 in CRC being approximately 400 pg/mL. For stages 1, 2, 3, and 4, the IL-6 levels were recorded as approximately 230, 282, 394, and 785 pg/mL, respectively [32]. Thus, serum-spiked IL-6 was quantified on the LSCF-GNP-modified IDME in the range of 0.1 to 3000 pg/mL. As shown in Figure 6(a), a clear increase in current responses was recorded for all IL-6 concentrations, indicating selective identification of IL-6 in human serum without any interference.

### 3.6. Specific IL-6 detection

Specific IL-6 detection experiments were performed with relative proteins namely CEA, TNF, complementary aptamer, and anti-IgG antibody. The CEA is the established biomarker for CRC and its over-expression is found in 95% of cases [33]. Further, the TNF cytokine is involved in various inflammatory processes. So these two molecules were chosen as the control proteins in the IL-6 biosensor. Apart from this, to confirm the specificity, a complementary aptamer was tested. As shown in Figure 6(b), there is no increment of current was noted with CEA, TNF, complementary aptamer, and anti-IgG antibody, which proved that the specific IL-6 detection on LSCF-GNP-modified IDME.

### 3.7. ELISA assay for IL-6 detection

To assess the efficiency of the IL-6 biosensor, the same functionalization was conducted on an ELISA polystyrene plate for IL-6 detection. ELISA is a well-established technique used to detect and screen various diseases. In the ELISA well, immobilization of the capture molecule plays a major role in target identification. In most cases, immobilization occurs through electrostatic interactions between biomolecules and the polystyrene ELISA well. However, this method may not be sufficient, as it can lead to instability and reduced biomolecular interactions. We evaluated our surface functionalization for aptamer immobilization and detected IL-6 using a sandwich assay. As shown in Figure 6(c), a clear increase in absorbance was noted with increasing IL-6 concentrations, and color changes in the ELISA well were visible

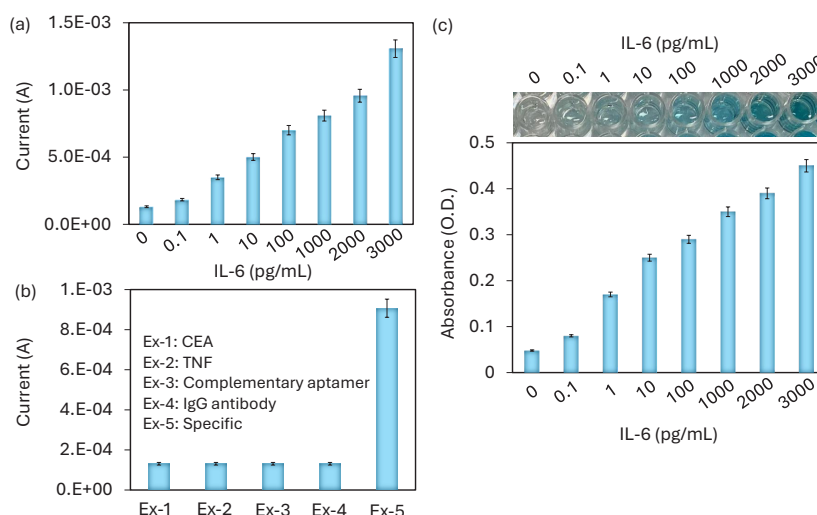


**Figure 6.** (a) IL-6 detection in serum-spiked samples. IL-6 was spiked into serum and detected using the IL-6 biosensor. Increases in current responses were recorded for all IL-6 concentrations, indicating selective identification of IL-6 in human serum without any interference. (b) Specific IL-6 detection. Specific IL-6 detection experiments were performed with relative proteins, namely Carcinoembryonic antigen (CEA), Tumour necrosis factor (TNF), complementary aptamer, and anti-IgG antibody. No increase in the current was noted with the control molecules. (c) Enzyme-linked immunosorbent assay (ELISA) assay for IL-6 detection. A clear increase in absorbance was observed with increasing IL-6 concentrations, and the color change in the ELISA wells was also visible starting from 1 pg/mL of IL-6.

starting from 1 pg/mL of IL-6. In both the IDME and electrochemical sensors, 0.1 pg/mL showed a slight increment of current response and the absorbance increment. At 1 pg/mL the current, the current response was doubled in IDME sensor and the visible detection from 1 pg/mL was observed in ELISA. The bigger response was obtained from 1 pg/mL in both cases. This consistency of the response was obtained through the stable immobilization of aptamer through the nanomaterials and enhanced the IL-6 interaction with its aptamer and antibody. Thus, the improved IL-6 biosensor has the potential to work effectively with any sensing surface without compromising the limit of detection.

#### 4. Conclusions

In conclusion, a highly sensitive IL-6 biosensor was developed for the early diagnosis of CRC. An aptamer and antibody were used to detect IL-6 on the IDME. Higher immobilization of the aptamer on the IDME was achieved by utilizing LSCF and GNPs. The current response to IL-6 increased with higher concentrations on the IDME using the aptamer-IL-6-antibody sandwich assay. IL-6 was detected in a range from 0.1 to 3000 pg/mL, with a limit of detection of 1 pg/mL. Additionally, the same current response was recorded with serum-spiked IL-6, indicating the selective detection of IL-6. Further control experiments with complementary aptamer, CEA, and TNF did not show any increase in current responses, confirming the specific detection of IL-6. Moreover, the same surface functionalization was demonstrated on the ELISA plate, resulting in the successful detection of IL-6. This biosensor, developed with LSCF and GNP, effectively detects low levels of IL-6 and aids in diagnosing CRC and its stages.

#### CRediT authorship contribution statement

**Rong Yan:** Data curation, Formal analysis, Investigation, Writing original draft preparation, **Thangavel LakshmiPriya:** Formal analysis, Writing-Reviewing and Editing, **Subash C.B. Gopinath:** Methodology, Conceptualization, Project administration, Funding acquisition, Resources, Writing-Reviewing and Editing, **Ismariza Ismail:** Data curation, Validation, Writing-Reviewing and Editing, **Sreeramanan Subramaniam:** Visualization, Writing-Reviewing and Editing, **Yeng Chen:** Validation, Writing-Reviewing and Editing, All are read and agreed with the content of manuscript.

#### Declaration of competing interest

The authors declare no competing interest.

#### Declaration of Generative AI and AI-assisted technologies in the writing process

The authors confirm that there was no use of artificial intelligence (AI)-assisted technology for assisting in the writing or editing of the manuscript and no images were manipulated using AI.

#### Acknowledgement

The study was funded by Natural Science Foundation of Shaanxi Province, China, 2022JQ-952.

#### References

- Motta, R., Cabezas-Camarero, S., Torres-Mattos, C., Riquelme, A., Calle, A., Figueroa, A., Sotelo, M.J., 2021. Immunotherapy in MSI metastatic colorectal cancer: current status and future perspectives. *Journal of Clinical and Translational Research* 7, 16. <https://doi.org/10.18053/jctres.07.202104.016>
- Zhang, X., Hu, F., Li, G., Li, G., Yang, X., Liu, L., Zhang, R., Zhang, B., Feng, Y., 2018. Human colorectal cancer-derived mesenchymal stem cells promote colorectal cancer progression through IL-6/JAK2/STAT3 signaling. *Cell Death and Disease* 9, 25. <https://doi.org/10.1038/s41419-017-0176-3>
- Buccafusca, G., Proserpio, I., Tralongo, A., Rametta Giuliano, S., Tralongo, P., 2019. Early colorectal cancer: Diagnosis, treatment and survivorship care. *Critical reviews in oncology/hematology* 136, 20-30. <https://doi.org/10.1016/j.critrevonc.2019.01.023>
- Tertis, M., Leva, P., Bogdan, D., Suci, M., Graur, F., Cristea, C., 2019. Impedimetric aptasensor for the label-free and selective detection of interleukin-6 for colorectal cancer screening. *Biosensors & Bioelectronics* 137, 123-132. <https://doi.org/10.1016/j.bios.2019.05.012>
- Wang, T., Song, P., Zhong, T., Wang, X., Xiang, X., Liu, Q., Chen, H., Xia, T., Liu, H., Niu, Y., Hu, Y., Xu, L., Shao, Y., Zhu, L., Qi, H., Shen, J., Hou, T., Fodde, R., Shao, J., 2019. The inflammatory cytokine IL-6 induces FRA1 deacetylation promoting colorectal cancer stem-like properties. *Oncogene* 38, 4932-4947. <https://doi.org/10.1038/s41388-019-0763-0>
- Lin, Y., He, Z., Ye, J., Liu, Z., She, X., Gao, X., Liang, R., 2020. Progress in understanding the IL-6/STAT3 pathway in colorectal cancer. *Oncotargets and Therapy* 13, 13023-13032. <https://doi.org/10.2147/OTT.S278013>
- Waldner, M.J., Foersch, S., Neurath, M.F., 2012. Interleukin-6 - A key regulator of colorectal cancer development. *International Journal of Biological Sciences* 8, 1248-1253. <https://doi.org/10.7150/ijbs.4614>
- Feng, S., Li, Z., Liu, M., Ye, Q., Xue, T., Yan, B., 2023. Postoperative serum interleukin-6 levels correlate with survival in stage I-III colorectal cancer. *BMC gastroenterology* 23, 156. <https://doi.org/10.1186/s12876-023-02800-9>
- Qiu, Z., Zhang, X., Jia, N., Li, X., Li, R., Gopinath, S.C.B., Jiao, M., 2023. Zeolite nanomaterial-modified dielectrode oxide surface for diagnosing Alzheimer's disease by dual molecular probed impedance sensor. *Turkish Journal of Biochemistry* 48, 668-674. <https://doi.org/10.1515/tjb-2023-0079>
- Gopinath, N., 2023. Artificial intelligence and neuroscience: An update on fascinating relationships. *Process Biochemistry (Barking, London, England)* 125, 113-120. <https://doi.org/10.1016/j.procbio.2022.12.011>

11. Taguchi, M., Ptitsyn, A., McLamore, E., Claussen, J., 2014. Nanomaterial-mediated biosensors for monitoring glucose. *Journal of Diabetes Science and Technology* **8**, 403-411. <https://doi.org/10.1177/1932296814522799>
12. Zhao, F., Wu, J., Ying, Y., She, Y., Wang, J., Ping, J., 2018. Carbon nanomaterial-enabled pesticide biosensors: Design strategy, biosensing mechanism, and practical application. *TrAC, Trends in Analytical Chemistry* **106**, 62-83. <https://doi.org/10.1016/j.trac.2018.06.017>
13. Jiang, C., Lan, L., Yao, Y., Zhao, F., Ping, J., 2018. Recent progress in application of nanomaterial-enabled biosensors for ochratoxin A detection. *TrAC, Trends in Analytical Chemistry* **102**, 236-249. <https://doi.org/10.1016/j.trac.2018.02.007>
14. LakshmiPriya, T., Fujimaki, M., Gopinath, S., Awazu, K., 2013. Generation of anti-influenza aptamers using the systematic evolution of ligands by exponential enrichment for sensing applications. *Langmuir* **29**, 15107-15115. <https://doi.org/10.1021/la4027283>
15. Hasanzadeh, M., Shadjou, N., de la Guardia, M., 2015. Iron and iron-oxide magnetic nanoparticles as signal-amplification elements in electrochemical biosensing. *TrAC, Trends in Analytical Chemistry* **72**, 1-9. <https://doi.org/10.1016/j.trac.2015.03.016>
16. Ali, A., Zafar, H., Zia, M., Ul Haq, I., Phull, A., Ali, J., Hussain, A., 2016. Synthesis, characterization, applications, and challenges of iron oxide nanoparticles. *Nanotechnol Sci Appl* **9**, 49-67. <https://doi.org/10.2147/NSA.S99986>
17. Soetaert, F., Korangath, P., Serantes, D., Fiering, S., Ivkov, R., 2020. Cancer therapy with iron oxide nanoparticles: Agents of thermal and immune therapies. *Advanced drug delivery reviews* **163-164**, 65-83. <https://doi.org/10.1016/j.addr.2020.06.025>
18. Thoidingjam, S., Tiku, A.B., 2017. New developments in breast cancer therapy: Role of iron oxide nanoparticles. *Advances in Natural Sciences: Nanoscience and Nanotechnology* **8**, 023002. <https://doi.org/10.1088/2043-6254/aa5e33>
19. Huang, Y., Zhang, L., Li, Z., Gopinath, S.C.B., Chen, Y., Xiao, Y., 2021. Aptamer-17 $\beta$ -estradiol-antibody sandwich ELISA for determination of gynecological endocrine function. *Biotechnology and Applied Biochemistry* **68**, 881-888. <https://doi.org/10.1002/bab.2008>
20. Luo, J., Gopinath, S.C.B., Subramaniam, S., Wu, Z., 2022. Arthritis biosensing: Aptamer-antibody-mediated identification of biomarkers by ELISA. *Process biochemistry (Barking, London, England)* **121**, 396-402. <https://doi.org/10.1016/j.procbio.2022.07.022>
21. LakshmiPriya, T., Horiguchi, Y., Nagasaki, Y., 2014. Co-immobilized poly(ethylene glycol)-block-polyamines promote sensitivity and restrict biofouling on gold sensor surface for detecting factor IX in human plasma. *The Analyst* **139**, 3977-85. <https://doi.org/10.1039/c4an00168k>
22. Gopinath, S., Balasundaresan, D., Akitomi, J., Mizuno, H., 2006. An RNA aptamer that discriminates bovine factor IX from human factor IX. *Journal of biochemistry* **140**, 667-76. <https://doi.org/10.1093/jb/mvj203>
23. Geng, H., Gopinath, S.C.B., Niu, W., 2023. Highly sensitive hepatitis B virus identification by antibody-aptamer sandwich enzyme-linked immunosorbent assay. *INNOSC Theranostics and Pharmacological Sciences* **5**, 7-14. <https://doi.org/10.36922/itps.298>
24. LakshmiPriya, T., Fujimaki, M., Gopinath, S., Awazu, K., Horiguchi, Y., Nagasaki, Y., 2013. A high-performance waveguide-mode biosensor for detection of factor IX using PEG-based blocking agents to suppress non-specific binding and improve sensitivity. *The Analyst* **138**, 2863-2870. <https://doi.org/10.1039/c3an00298e>
25. Gopinath, S., LakshmiPriya, T., Awazu, K., 2014. Colorimetric detection of controlled assembly and disassembly of aptamers on unmodified gold nanoparticles. *Biosensors & Bioelectronics* **51**, 115-123. <https://doi.org/10.1016/j.bios.2013.07.037>
26. Spiridonova, V.A., Novikova, T.M., Snigirev, O.V., 2016. Obtaining DNA aptamers to human interleukin-6 for biomagnetic immunoassay nanosensors. *Moscow University Physics Bulletin* **71**, 135-138. <https://doi.org/10.3103/S002713491601015X>
27. Guo, S., LakshmiPriya, T., Gopinath, S., Anbu, P., Feng, Y., 2019. Complementation of ELISA and an interdigitated electrode surface in gold nanoparticle functionalization for effective detection of human blood clotting defects. *Nanoscale Research Letters* **14**, 222. <https://doi.org/10.1186/s11671-019-3058-z>
28. Qiu, Z., Shen, Q., Jiang, C., Yao, L., Sun, X., Li, J., Duan, C., Li, R., Li, X., Gopinath, S.C.B., Anbu, P., LakshmiPriya, T., Li, X., 2021. Alzheimer's disease determination by a dual probe on gold nanourchins and nanohorn hybrids. *International Journal of Nanomedicine* **16**, 2311-2322. <https://doi.org/10.2147/IJN.S302396>
29. Mat Zaid, M., Che-Engku-Chik, C., Yusof, N., Abdullah, J., Othman, S., Issa, R., Md Noh, M., Wasoh, H., 2020. DNA electrochemical biosensor based on iron oxide/Nanocellulose crystalline composite modified screen-Printed carbon electrode for detection of mycobacterium tuberculosis. *Molecules* **25**, 3373. <https://doi.org/10.3390/molecules25153373>
30. Chen, Y.C., Chou, Y.C., Chang, J.H., Chen, L.T., Huang, C.J., Chau, L.K., Chen, Y.L., 2021. Dual-functional gold-iron oxide core-satellite hybrid nanoparticles for sensitivity enhancement in biosensors: Via nanoplasmonic and preconcentration effects. *The Analyst* **146**, 6935-6943. <https://doi.org/10.1039/d1an01334c>
31. Zhao, J., Chang, W., Liu, L., Xing, X., Zhang, C., Meng, H., Gopinath, S., LakshmiPriya, T., Chen, Y., Liu, Y., 2021. Graphene oxide-gold nanoparticle-aptamer complexed probe for detecting amyloid beta oligomer by ELISA-based immunoassay. *Journal of Immunological Methods* **489**, 112942. <https://doi.org/10.1016/j.jim.2020.112942>
32. Esfandi, F., Mohammadzadeh Ghobadloo, S., Basati, G., 2006. Interleukin-6 level in patients with colorectal cancer. *Cancer letters* **244**, 76-78. <https://doi.org/10.1016/j.canlet.2005.12.003>
33. Wang, C., Xin, D., Yue, Q., Wan, H., Li, Q., Wang, Y., Wu, J., 2023. A novel electrochemical IL-6 sensor based on au nanoparticles-modified platinum carbon electrode. *Frontiers in Bioengineering and Biotechnology* **11**, 1128934. <https://doi.org/10.3389/fbioe.2023.1128934>
34. Diacci, C., Burtscher, B., Berto, M., Ruoko, T., Lienemann, S., Greco, P., Berggren, M., Borsari, M., Simon, D., Bortolotti, C., Biscarini, F., 2024. Organic electrochemical transistor aptasensor for interleukin-6 detection. *ACS Applied Materials & Interfaces* **16**, 61467-61474. <https://doi.org/10.1021/acsami.3c12397>
35. Adrover-Jaume, C., Alba-Patiño, A., Clemente, A., Santopolo, G., Vaquer, A., Russell, S., Barón, E., González Del Campo, M., Ferrer, J., Berman-Riu, M., García-Gasalla, M., Aranda, M., Borges, M., de la Rica, R., 2021. Paper biosensors for detecting elevated IL-6 levels in blood and respiratory samples from COVID-19 patients. *Sensors and actuators. B, Chemical* **330**, 129333. <https://doi.org/10.1016/j.snb.2020.129333>
36. Cancelliere, R., Cosio, T., Campione, E., Corvino, M., D'Amico, M., Micheli, L., Signori, E., Contini, G., 2023. Label-free electrochemical immunosensor as a reliable point-of-care device for the detection of interleukin-6 in serum samples from patients with psoriasis. *Frontiers in Chemistry* **11**, 1251360. <https://doi.org/10.3389/fchem.2023.1251360>
37. Munje, R., Muthukumar, S., Jagannath, B., Prasad, S., 2017. A new paradigm in sweat based wearable diagnostics biosensors using room temperature ionic liquids (RTILs). *Scientific Reports* **7**, 1950. <https://doi.org/10.1038/s41598-017-02133-0>
38. Rahman, M., Pal, R., Islam, N., Freeman, R., Berthiaume, F., Mazzeo, A., Ashraf, A., 2023. A facile graphene conductive polymer paper based biosensor for dopamine, TNF- $\alpha$ , and IL-6 detection. *Sensors (Basel)* **23**, 8115. <https://doi.org/10.3390/s23198115>
39. Huang, J., Chen, H., Niu, W., Fam, D.W.H., Palaniappan, A., Larisika, M., Faulkner, S.H., Nowak, C., Nimmo, M.A., Liedberg, B., Tok, A.I.Y., 2015. Highly manufacturable graphene oxide biosensor for sensitive Interleukin-6 detection, RSC *Advances* **5**, 39245-39251. <https://doi.org/10.1039/c5ra05854f>